Computer Methods and Programs in Biomedicine 249 (2024) 108138

Contents lists available at ScienceDirect

Computer Methods and Programs in Biomedicine

journal homepage: www.sciencedirect.com/journal/computer-methods-and-programs-in-biomedicine

Patient-specific left atrium contraction quantification associated with atrial fibrillation: A region-based approach

Sachal Hussain [a,*], Matteo Falanga [a], Antonio Chiaravalloti [b], Corrado Tomasi [b], Cristiana Corsi [a]

[a] DEI, Cesena Campus, University of Bologna, Italy
[b] Santa Maria delle Croci Hospital, AUSL della Romagna, Ravenna, Italy

ARTICLE INFO

Keywords:
Left atrium regionalization
Atrial fibrillation
Atrial mechanical function
Regional analysis

ABSTRACT

Background and objectives: Atrial fibrillation (AF) is a widespread cardiac arrhythmia that significantly impacts heart function. AF disrupts atrial mechanical contraction, leading to irregular, uncoordinated, and slow blood flow inside the atria which favors the formation of clots, primarily within the left atrium (LA). A standardized region-based analysis of the LA is missing, and there is not even any consensus about how to define the LA regions. In this study we propose an automatic approach for regionalizing the LA into segments to provide a comprehensive 3D region-based LA contraction assessment. LA global and regional contraction were quantified in control subjects and in AF patients to describe mechanical abnormalities associated with AF.
Methods: The proposed automatic approach for LA regionalization was tested in thirteen control subjects and seventeen AF patients. After dividing LA into standard regions, we evaluated the global and regional mechanical function by measuring LA contraction parameters, such as regional volume, global and regional strains, regional wall motion and regional shortening fraction.
Results: LA regionalization was successful in all study subjects. In the AF group compared with control subjects, results showed: a global impairment of LA contraction which appeared more pronounced along radial and circumferential direction; a regional impairment of radial strain which was more pronounced in septal, inferior, and lateral regions suggesting a greater reduction in mechanical efficiency in these regions in comparison to the posterior and anterior ones.
Conclusion: An automatic approach for LA regionalization was proposed. The regionalization method was proved to be robust with several LA anatomical variations and able to characterize contraction changes associated with AF.

1. Introduction

Left atrium (LA) is a complex structure and plays a crucial mechanical role in modulating left ventricle (LV) filling, acting as a reservoir during systolic phase, as a conduit during early diastolic phase, and as a booster pump during late diastolic phase [1]. It is well known that abnormalities in LA mechanical function favour clot formation due to inadequate contraction, disturbed blood flow and incomplete blood washout in the left atrial appendage (LAA) [2]. Atrial fibrillation (AF) is considered one of the epidemic of our century [3]. Fundamental epidemiological studies on AF carried out in developed nations between the late 20th century and the early 21st century, estimated that AF prevalence in the general population ranges from 0.5% to 1% [4,5]. Nevertheless, in recent years, leading opinions have pointed to a considerably higher figure, if hospitalizations, emergency room and outpatients non-urgent visits related to AF are taken into account [6,7],. AF basically disrupts LA and LAA mechanics, leading to LA dilation, electrical and tissue modifications and long-term structural abnormalities often lasting well over sinus rhythm (SR) restoration. Atrial dilation per se, which appears at an early stage during AF, has been demonstrated to be associated with an increased cardiovascular morbidity and mortality [8,9].

Significant impairment of the LA strains has been described in several disorders [10,11], and in AF a decrease in left atrial ejection fraction has been widely reported [12]. However, a standardized region-based analysis able to (1) maintain consistency with accepted anatomic data, (2) utilize accepted approaches to LA segmentation and nomenclature and (3) allow precise localization by using anatomic landmarks, is still lacking, and even any consensus about how to define

* Corresponding author.
E-mail address: sachal.hussain3@unibo.it (S. Hussain).

https://doi.org/10.1016/j.cmpb.2024.108138
Received 15 December 2023; Received in revised form 17 March 2024; Accepted 18 March 2024
Available online 19 March 2024

List of acronyms

LA/LV	Left Atrium/Left Ventricle
LAA	Left Atrial Appendage
AF	Atrial Fibrillation
SR	Sinus Rhythm
CTRL	Control subjects
PVs	Pulmonary Veins
MV	Mitral Valve
LS/RS	Left/Right Superior
LI/RI	Left/Right Inferior
EF	Ejection Fraction
REF	Regional Ejection Fraction
IA	Index of Asynchrony
LS	Longitudinal Strain
RS	Radial Strain
RRD	Regional Radial Dimension
RRS	Regional Radial Strain
CS	Circumferential Strain
RWM	Regional Wall Motion
RSF	Regional Shortening Fraction
CFEs	Complex Fractionated Electrograms
2DSTE/3DSTE	2D/3D speckle tracking echocardiography

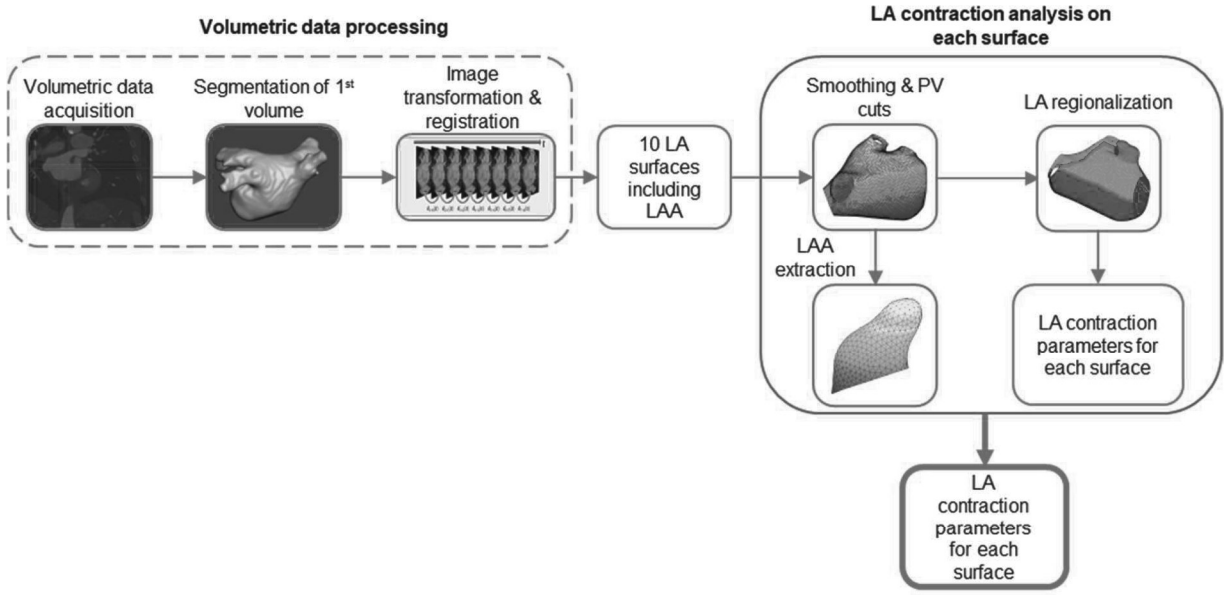

Fig. 1. Schematic diagram of the implementation of LA regionalization and evaluation of contraction parameters in a complete cardiac cycle.

the regions of the LA has yet to be made. The first consequence of this lacuna is the difficulty in comparing results from different studies which apply different approaches for region-based LA segmentation. The method so far currently adopted for region definition, is the surface flattening method [13] and it seems to have some limitations; authors reported that some LA intrinsic structures such as the pulmonary veins (PVs), mitral valve (MV) and LAA may cause a distorting effect on the flattening process of the LA surface [14]. Moreover, other fairly common anatomical variations, for instance in the number and size of PVs [15], can make this method more challenging to use.

A shared and standardized method for regional assessment of LA would aid the study of several functional issues such as: the detection of more subtle AF-related damages in different regions; the regional contributions to the global LA contractile impairment; the correlation between propagation and amplitude of EGM abnormalities and regional contraction; the assessment of regional impacts of medical and catheter-based therapies on mechanics, both in SR and during AF. Finally, by means of a quantitative approach it would be possible to continuously monitor regional function and remodelling, following catheter ablation [16]. For research purposes, the quantification of AF contraction on a patient-specific basis could provide realistic boundary conditions for computational fluid-dynamics simulations, a promising tool for analysing intra-atrial blood flow and its correlations with stroke risk associated with AF.

In this study, we propose an automatic approach for regionalizing the LA into segments to provide a comprehensive 3D region-based LA contraction assessment, which is to date available only through echo imaging in 2D. To this aim, we analysed LA global and regional contraction in control subjects and in AF patients and described mechanical abnormalities associated with AF.

2. Materials and methods

2.1. Selection of patients and CT imaging

Study data were acquired within the FATA project approved by the Ethics Committee of the Romagna Heath Authority (CEROM), in Italy (CEIIAV n. 1456 prot.6076/2015 I.5/220). All subjects gave written informed consent in accordance with the Declaration of Helsinki.

The enrolment was retrospective and consisted of twelve patients with paroxysmal AF (10 males, mean age: 58.7 $\pm$ 10.5 yrs and 2 females, mean age: 74 $\pm$ 3.0 yrs); five patients with persistent AF (3 males, mean age: 60.6 $\pm$ 4.0 yrs and 2 females, mean age: 73.5 $\pm$ 1.5 yrs); thirteen control subjects (CTRL) without any previous history of AF and no evidence of cardiac structural disease (10 males, mean age: 60 $\pm$ 10.2 yrs and 3 females, mean age: 61.5 $\pm$ 0.5 yrs)

Cardiac CT dynamic acquisitions after injection of contrast medium were obtained applying retrospective ECG gating during normal SR

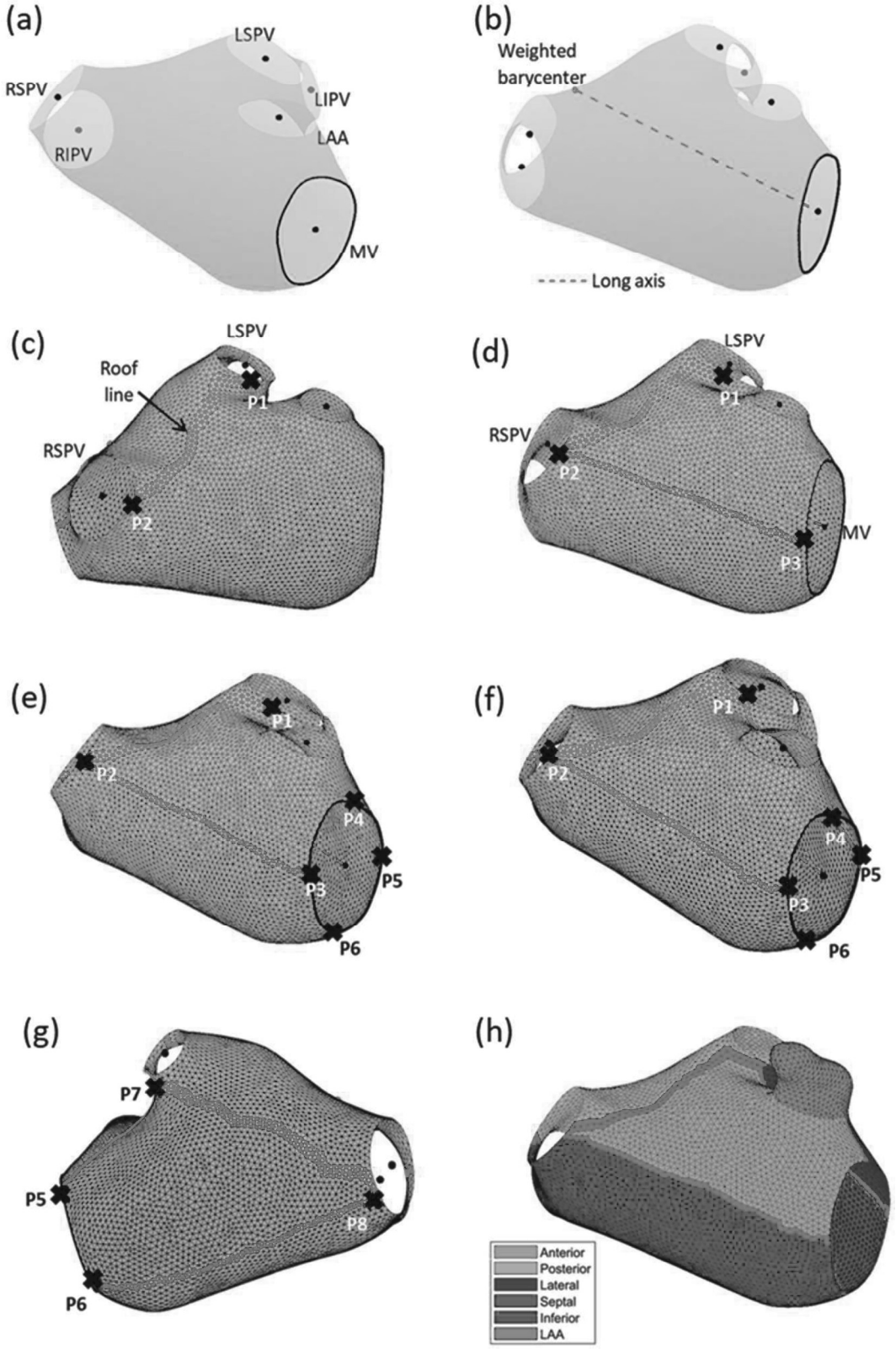

Fig. 2. Graphical description of the LA regionalization approach. (a) LA surface showing the 4 PVs and the MV and their respective barycenters; (b) long axis detection obtained connecting the barycenter of the MV and the weighted barycenter of the PVs; (c) detection of the roof boundary line between the superior PVs; (d) detection of the starting point on the mitral annulus by linking the MV barycenter and the point on the previously computed RSPV ostium; (e) the four points on MV annulus obtained by 90° rotation of the starting point; (f) connection of all the four points with the nearby PVs; (g) boundaries of the posterior and inferior regions generated by connecting the points on the MV and the inferior PVs; (h) final LA segmentation into regions.

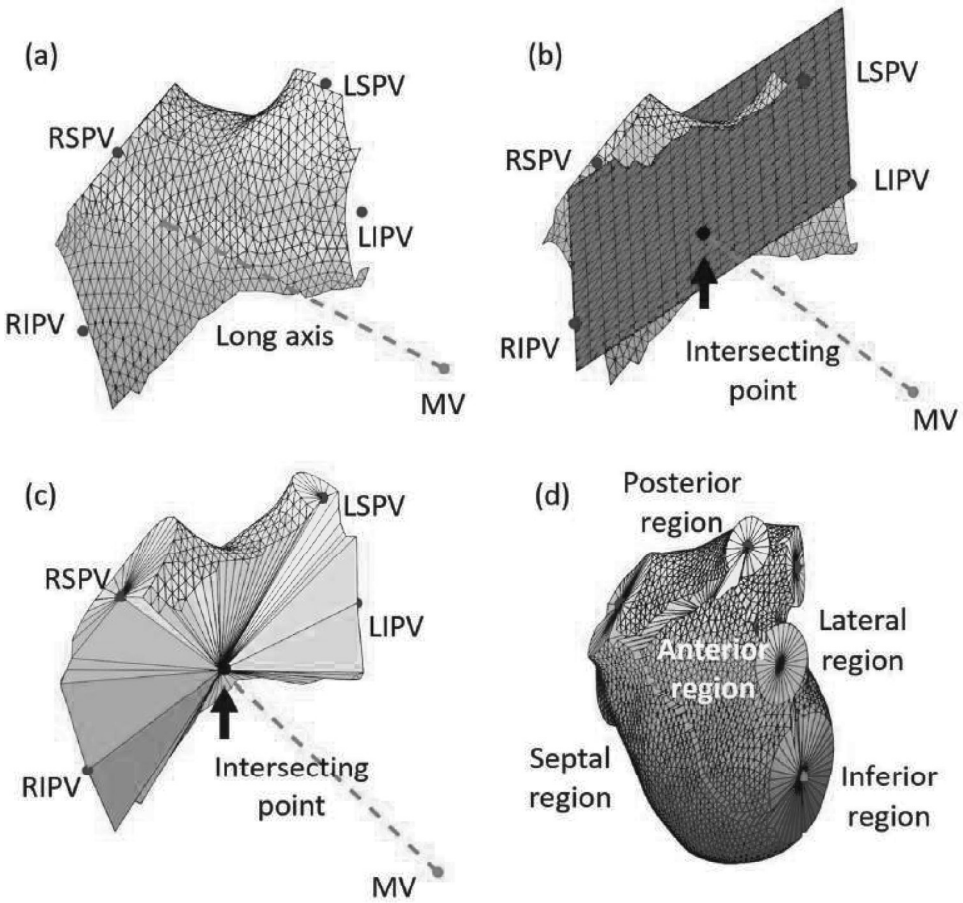

Fig. 3. Graphical description of the LA volumetric regions. (a) the posterior surface and long axis of LA; (b) best fitting cutting plane used to detect the intersecting point with LA long axis; (c) closed posterior region obtained by connecting all the posterior boundary points with the intersecting point; (d) final five closed regions of LA.

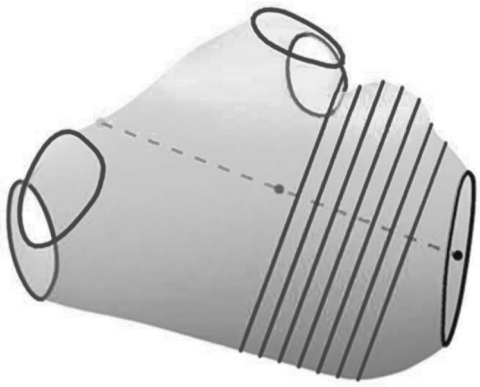

Fig. 4. Six equally distributed circumferential curves on LA surface starting from midpoint of long axis to MV barycenter.

using a 64-slice multi-detector CT scanner (Philips Brilliance 64 CT scanner) in each patient.

Volumetric CT images were reconstructed for a total of 10 phases from ventricular end diastole (from 0%RR to 90%RR, where RR indicates the interval between two consecutive electrocardiographic R wave peaks). Each reconstructed CT volume was 512 × 512 × 200 pixels. The voxel resolution was not isotropic: in-plane resolution was 0.39 mm, and through-plane resolution was 1 mm, resulting in a voxel size of $0.39 \times 0.39 \times 1$ mm^3.

2.2. Data analysis

2.2.1. Image segmentation and post-processing

For LA segmentation in our cohort, an active contour algorithm [17] was implemented in MATLAB (MATLAB R2023a, The Mathworks Inc.). The active contour model we applied is based on Mumford-Shah segmentation techniques and level set models: an energy-based functional taking into account mean gray level intensity inside and outside the evolving contour and a regularization term is minimized partitioning the image in the two most different regions in terms of average gray level. After the selection of a volume of interest within the CT scan and the manual positioning of a seed point inside the LA, the algorithm was applied to the first CT volume. The LA surface resulting from segmentation included proximal regions of the PVs, MV and part of the basal region of the left ventricle and the LAA.

The workflow for the analysis of CT data is shown in Fig. 1 and its several steps are detailed in the following subsections.

After finalizing the segmentation process, the deformation of the LA surface throughout the cardiac cycle was computed by applying a 3D image registration step to the CT volumes. The registration of CT volumes required two steps: a preliminary rigid transformation followed by a nonrigid transformation based on B-spline [13] using the mean square difference as a similarity measure. Following the registration procedure, the displacements between frames were then applied to the vertices of the LA surface allowing the reconstruction of the LA surfaces for the remaining phases [14].

Before regionalization, a Laplacian smoothing was applied to the LA surfaces and cutting planes were defined on the surface extracted from

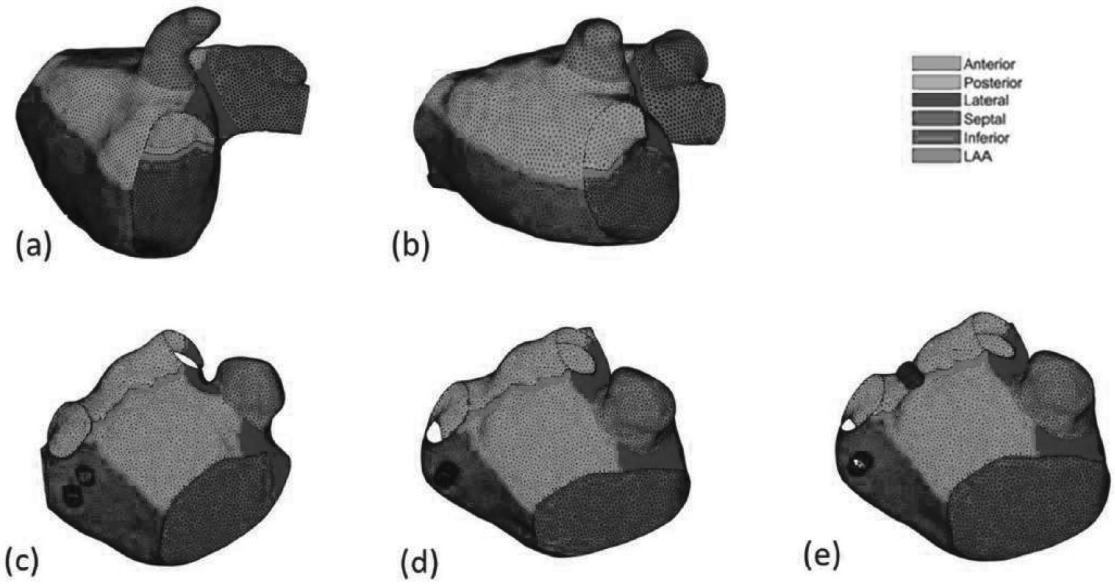

Fig. 5. Regionalization results on anatomically variable LA geometries: (a) long trunk; (b) short trunk; (c) double middle PVs; (d) middle PV; (e) top-middle PV.

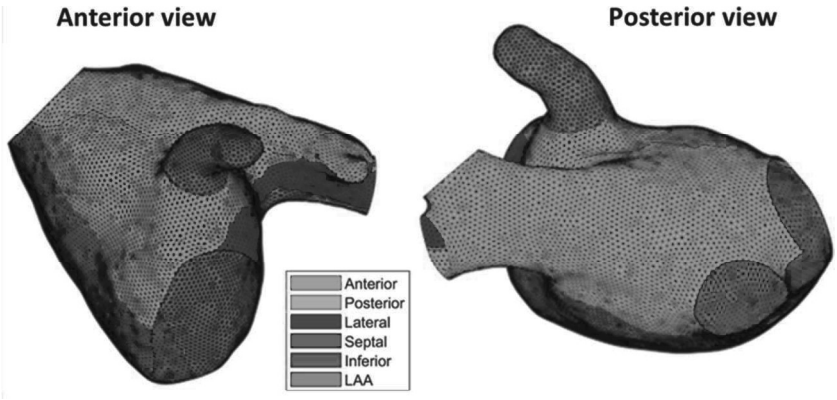

Fig. 6. Regionalization result in one anatomy in which the performance of the proposed approach was considered poor.

the first volume, to detect the four PVs ostia, the MV and the LAA (taking into account the curvature of the surface and including the ridge within the LA chamber). For this purpose, open-source Autodesk Meshmixer software [18] was utilized. The cut planes were then propagated to all the surfaces throughout the cardiac cycle.

2.2.2. LA regionalization

To initiate the process of regionalization, the annulus of MV, LAA, and PVs ostia were automatically recognized according to their respective location and area. Then the barycenter of each ostium was computed by using the coordinates of the points on the ostia (Fig. 2(a)). Subsequently, the weighted barycenter of the four PVs was calculated by taking into consideration the area of the ostium of each PV and their corresponding barycenter. In case of more than four PVs, the extra PV(s) was identified by considering the smaller size of its ostium and discarded.

In the next step, the long axis of LA was defined by connecting the weighted barycenter of the PVs and MV barycenter with a straight line (Fig. 2(b)). In our approach, the long axis was considered as a reference to compute contraction parameters and for the projection of boundary lines onto the LA body.

Following the detection of the LA long axis, a line was drawn to connect the left superior (LS) pulmonary vein and the right superior (RS) pulmonary vein barycenter: this line intersects the two ostia and consequently one point on LS and on the RSPV ostium were detected; these two points were rotated 90° towards the MV (P1 and P2 in Fig. 2 (c)). Finally, by connecting P1 and P2 onto the surface of LA, the roof line was generated - a borderline between anterior and posterior regions (roof line, Fig. 2(c)). Similarly, the left inferior (LI) pulmonary vein barycenter was linked with the LS pulmonary vein barycenter; and the right inferior (RI) pulmonary vein barycenter was linked with the RS barycenter. These lines were projected onto the LA surface in the direction of midpoint of long axis and used as boundaries between lateral and posterior regions and between septal and posterior regions, respectively.

In the next step, the MV anulus was divided into four segments: the MV barycenter was linked with P2; this segment was projected on the LA surface to detect point P3 on the MV annulus (Fig. 2(d)); P3 was then rotated three times at 90° in the clockwise direction to get three more points, namely P4, P5 and P6 (Fig. 2(e)). Then, P4 was joined with P1 and P3 with P2 (Fig. 2(f)); then P5 and P6 were joined with the barycenter of LI and RI respectively (Fig. 2(f)). By connecting P5 and P6 with the barycenter of LI and RI respectively, another point was generated on each PV, namely P7 and P8 (Fig. 2(g)). The boundary between inferior and posterior zones was defined by linking P7 and P8 at the ostium of LI and RI, respectively. The complete surface regionalization of LA yielded five regions: anterior, posterior, lateral, septal, and inferior (Fig. 2(h)).

Once the surface regionalization was obtained, the posterior region

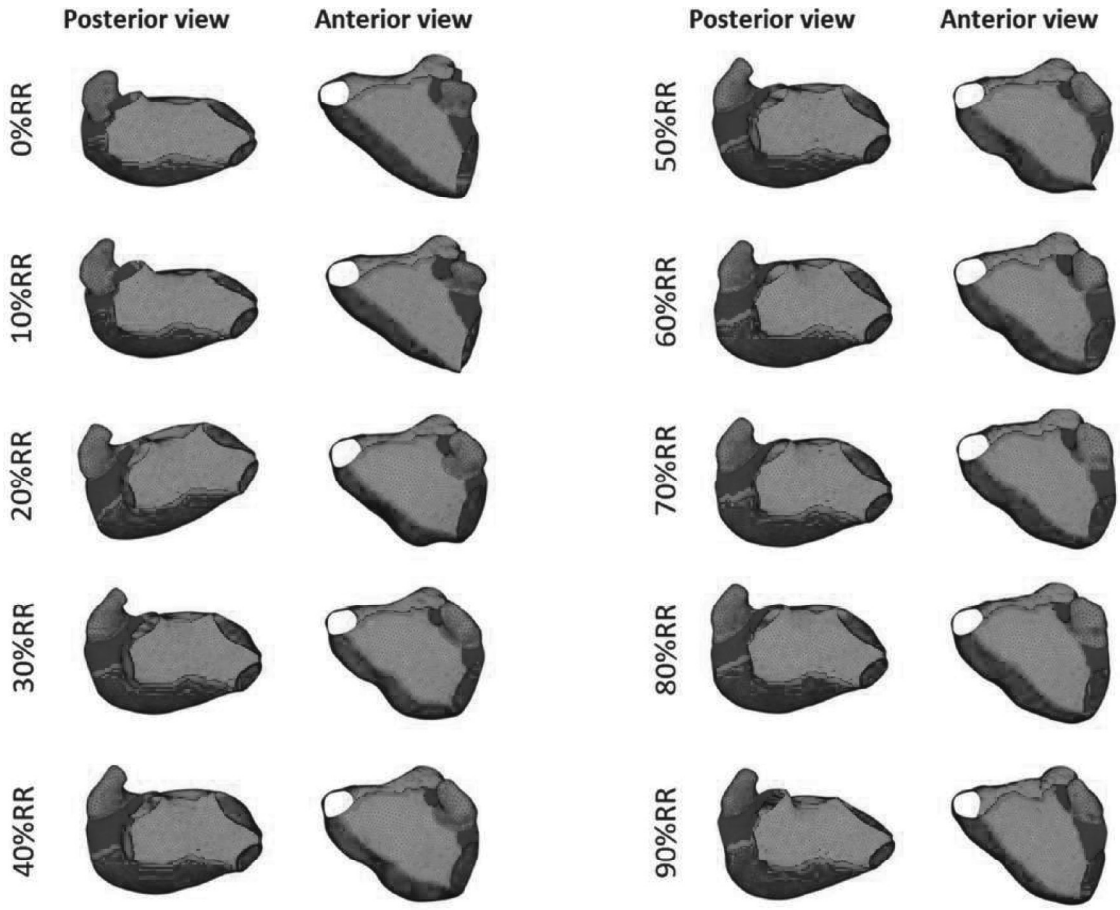

Fig. 7. Regionalization results applied to the ten surfaces throughout the cardiac cycle (from 0%RR to 90%RR, where RR indicates the interval between two consecutive electrocardiographic R wave peaks) in one sample patient.

and the long axis were selected to detect volumetric regions (Fig. 3(a)). By using the barycenter of each PV, the best fitting plane was computed. This best fitting plane intersected the long axis at one point, named as intersecting point (Fig. 3(b)). To close posterior region, all the boundary points of posterior region were projected towards the intersecting point (Fig. 3(c)); this closing was repeated for each surface in the cardiac cycle to compute posterior regional volumetric curve. For all the other regions, all the boundary points were projected onto the long axis (Fig. 3 (d)). This complete implementation is graphically described in Fig. 3.

This entire regionalization analysis was repeated for each of the 10 surfaces throughout the cardiac cycle resulting in posterior, lateral, inferior, anterior, and septal dynamic volumetric regions (Fig. 1).

2.3. Testing and statistics

2.3.1. LA regionalization in presence of anatomical variations

The proposed LA regionalization approach was confronted with well-established variants of LA-PV structures to test its capability to work on different LA anatomies, [19,20],. The regionalization of the most common four-PV anatomy is presented in Fig. 2(h). Other variants were dealt with: in anatomies with ipsilateral superior and inferior PVs very close to each other forming either short or long trunks, the trunk part was manually excluded and then regionalization was applied. In other well-known existing variants, not represented in our dataset, such as short trunk, long trunk, middle PV, double mid PVs, and top-middle PV, we chose to generate the relative cases virtually. Thirty CT volumes presenting a wide range of anatomical variations (short trunk, long trunk, middle PV, double mid PVs, and top-middle PV) were tested.

The performance of our regionalization method was evaluated qualitatively by an expert electrophysiologist who assigned a grade to each regionalization result (good - fair - poor - unacceptable) based on experience. Only one surface for each case was evaluated, corresponding to the first CT volume, and a total of 30 individual surface-case were evaluated by the EP specialist.

2.3.2. LA contraction parameters computation

Parameters to assess global LA function were computed, including LA volume-time curve and LA ejection fraction (EF).

To study regional changes, region-based contraction parameters were defined. Regional volumes were computed throughout the cardiac cycle as well as regional EF (REF) for each region. From regional volumetric curves, REF was computed by considering end-diastolic and end-systolic atrial phases from LA volumetric curve. For each region, the standard deviation (SD) of the time intervals at which regional volumes reached the peak value was computed and was used as an index of LA asynchrony (IA) in each patient [21].

Furthermore, to conduct strain analysis, longitudinal strain (LS) was computed by tracing the variation in the length of the long axis referring to the end-diastolic ventricular frame throughout the cardiac cycle, using this formula:

$$\mathrm{LS(x)} = \frac{\mathrm{LA_{len}(x) - LA_{len\_ED}}}{\mathrm{LA_{len\_ED}}} \cdot 100$$

where $\mathrm{LA_{len}(x)}$ is the length of long axis at current frame x and $\mathrm{LA_{len\_ED}}$ is the length of long axis at end-diastolic ventricular frame.

To analyze radial strain (RS), regional radial dimension (RRD) was evaluated for each region, as the average of the Euclidean distance of each vertex of that specific region from the long axis and then regional

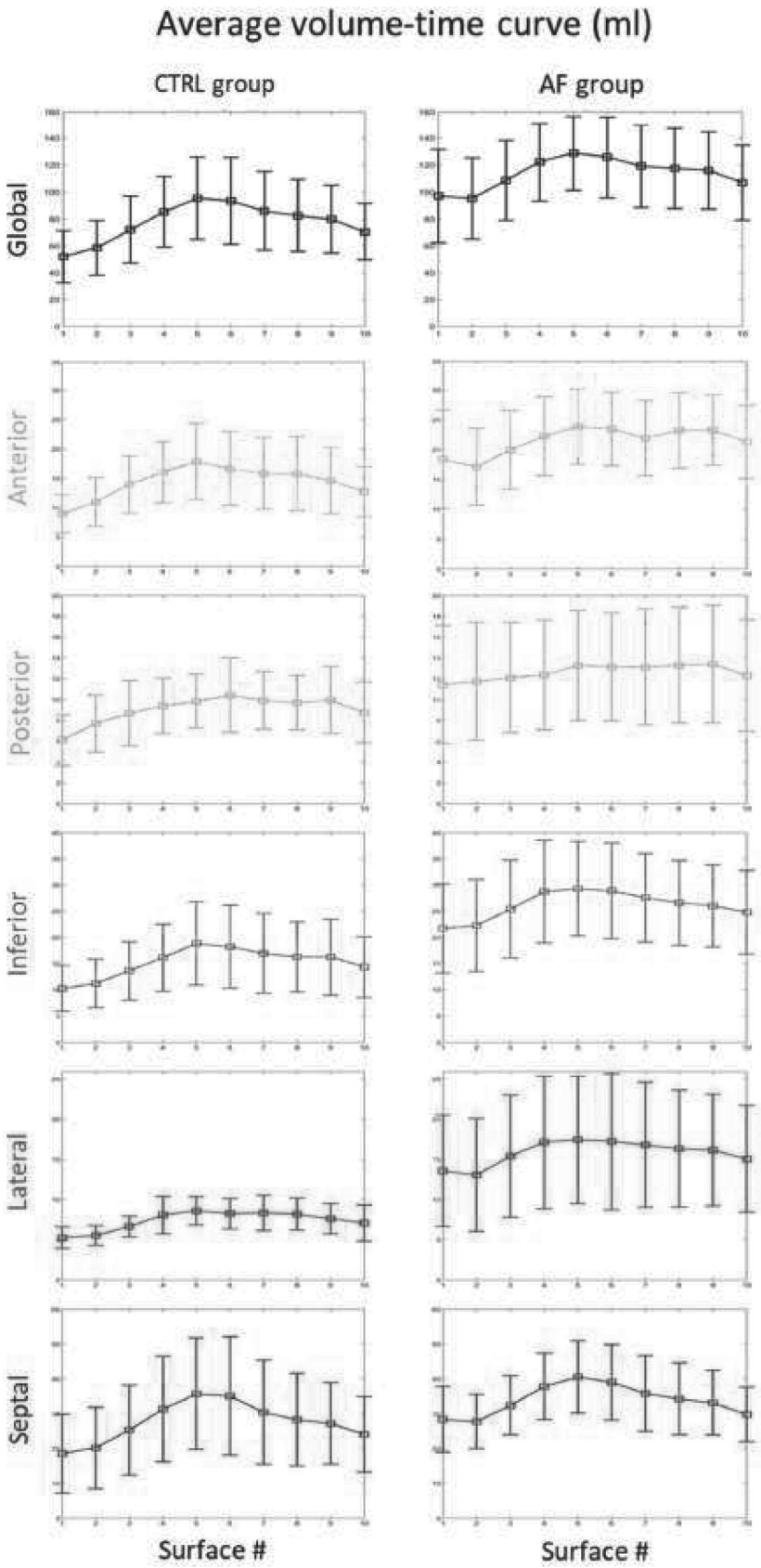

Fig. 8. Mean LA and regional volumetric curves throughout the cardiac cycle in CTRL (left panels) and AF (right panels) groups with standard deviation.

Table 1
Computed parameters in CTRL and AF groups.

Parameters		CTRL group ($n = 13$)		AF group ($n = 17$)		p-value
		Mean +/- SD	Range	Mean +/- SD	Range	
Mean volume (ml)	**LA**	77.6 +/- 13.5	[52, 95.5]	113.8 +/- 10.9	[95.3, 129]	$P < 0.005$
	Anterior	14.3 +/- 2.6	[9.0, 17.8]	21.5 +/- 2.2	[17.1, 23.8]	$P < 0.005$
	Posterior	9.1 +/- 1.2	[6.1. 10.4]	12.6 +/- 0.7	[11.4, 13.4]	$P < 0.005$
	Inferior	15.2 +/- 2.7	[10.2, 18.8]	26.1 +/- 2.5	[21.7, 29.3]	$P < 0.005$
	Lateral	7.4 +/- 1.1	[5.3, 8.6]	15.9 +/- 1.5	[13.1, 17.5]	$P < 0.005$
	Septal	27.6 +/- 5.5	[18.5, 35.7]	33.9 +/- 4.2	[27.8, 40.5]	$P = 0.01$
IA regional volume		1.2	[0.5, 2.8]	1.5	[0.5, 2.8]	$P = 0.20$
Peak LS (%)		22 +/- 7.9	[11.0, 44.3]	13.7 +/- 7.8	[3.6, 29.2]	$P = 0.01$
Peak RS (%)		25.2 +/- 11	[13.9, 60.5]	11.7 +/- 7.7	[2.0, 26.1]	$P < 0.005$
Peak CS (%)		30.1 +/- 11	[12.8, 55.2]	13.1 +/- 7.6	[2.7, 28.7]	$P < 0.005$
Peak RRS (%)	**Anterior**	32.8 +/- 19.6	[10.8, 92.2]	14.6 +/- 12.3	[0, 34.1]	$P = 0.01$
	Posterior	20.2 +/- 15.7	[3.1, 68.2]	14.5 +/- 8.3	[0.8, 26.4]	$P = 0.26$
	Inferior	28.2 +/- 9.1	[15.2, 51.6]	15.8 +/- 8.4	[3.2, 31.0]	$P < 0.005$
	Lateral	24.3 +/- 7.9	[11, 36.9]	13.7 +/- 8.1	[3.3, 30.5]	$P < 0.005$
	Septal	29.0 +/- 13.5	[13, 69.4]	13.1 +/- 8.6	[0.3, 28.5]	$P < 0.005$
Peak RWM (mm)	**Anterior**	5.2 +/- 2.5	[2.1, 13.0]	2.8 +/- 2.2	[0, 6.2]	$P = 0.01$
	Posterior	2.6 +/- 1.6	[0.5, 7.2]	2.3 +/- 1.3	[0.2, 4.3]	$P = 0.69$
	Inferior	5.0 +/- 1.7	[2.3, 8.6]	3.5 +/- 1.7	[0.9, 7.0]	$P = 0.02$
	Lateral	4.0 +/- 1.3	[2.0, 6.1]	2.9 +/- 1.5	[0.9, 6.2]	$P = 0.04$
	Septal	6.5 +/- 2.6	[3.1, 14.3]	3.5 +/- 2.3	[0.08, 6.6]	$P < 0.005$
IA_{RWM}		1.1	[0, 2.1]	1.6	[0, 3.1]	$P = 0.08$
RSF	**Anterior**	0.2 +/- 0.09	[0.1, 0.5]	0.1 +/- 0.09	[0, 0.3]	$P < 0.005$
	Posterior	0.2 +/- 0.09	[0.03, 0.4]	0.1 +/- 0.06	[0.01, 0.2]	$p = 0.27$
	Inferior	0.2 +/- 0.05	[0.1, 0.3]	0.1 +/- 0.06	[0.03, 0.2]	$P < 0.005$
	Lateral	0.2 +/- 0.05	[0.1, 0.3]	0.1 +/- 0.06	[0.03, 0.2]	$P < 0.005$
	Septal	0.2 +/- 0.07	[0.1, 0.4]	0.1 +/- 0.07	[0, 0.2]	$P < 0.005$

radial strain (RRS) was calculated as:

$$RRS(x) = \frac{RRD(x) - RRD_{ED}}{RRD_{ED}} \cdot 100$$

where RRD(x) is the current regional radial dimension of any region and RRD_{ED} is the regional radial dimension at ventricular end-diastole of that same region. Ultimately, RS is the average of all RRS values at each frame.

To calculate circumferential strain (CS), six circumferential curves (Fig. 4) were considered between the midpoint of long axis and the MV barycenter. These curves were equidistantly distributed and for each curve [22], the percentage strain was computed using the formula:

$$CS(x) = \frac{L(x) - L_{ED}}{L_{ED}} \cdot 100$$

where L(x) is the length of the curve at frame x and L_{ED} is the length of the curve at end-diastolic ventricular frame. The circumferential strain of LA was calculated as the average strain of those six curves.

Once global strains were computed, the contraction of each region was assessed in terms of regional wall motion (RWM), calculated as the difference between current RRD and RRD at ventricular end diastole for each region:

$$RWM(x) = RRD(x) - RRD_{ED}$$

According to this definition, regional wall motion equals zero at ventricular end diastole. The index of LA asynchrony (IA_{RWM}) for each region was computed also for the regional wall motion curves as the standard deviation (SD) of the time intervals at which RWM curves reached the peak value [18].

To calculate regional shortening fraction (RSF) for each surface region, the corresponding regional peak wall motion was divided by the corresponding peak radial dimension. RSF values were then averaged for each subject.

2.3.3. Global and regional assessment in controls and AF patients

The procedure developed for LA regionalization and for the computation of the proposed indices was tested in 17 patients with AF and 13 control subjects. All surfaces are available in the Zenodo repository (10.5281/zenodo.10579450).

Global and regional average LA volume-time curves were compared between AF and CTRL groups, as well as EF and REF. Average IA in the two groups was computed and compared between them.

The same comparison was performed between longitudinal, radial, and circumferential strains computed for the LA chamber and for RRS in each region in the two groups in terms of peak strains. Peak RWM and RSF were also compared.

2.3.4. Statistical analysis

Data are expressed as mean ± standard deviation. T-test was applied to verify the statistically significant difference between the two groups with $p < 0.05$.

3. Results

3.1. Anatomical variations

Fig. 5 shows the LA regionalization obtained by applying the proposed approach, in five samples of anatomies categorized according to the following PVs anatomical variations: long trunk, short trunk, double middle PVs, middle PV, top-middle PV.

To assess the reliability of our approach in a clinical setting, an expert electrophysiologist visually graded the quality of our regional segmentation as being good in 20 cases, fair in 7 and poor in 3 cases.

One case out of the 3 classified as poor is shown in Fig. 6 as an example of an unsatisfactory regional regionalization.

3.2. Contraction in control subjects and AF patients

Examples of regional segmentation and dynamic detection of regions are shown in Fig. 7. Regional segmentation was performed throughout the complete cardiac cycle, capturing both systole and diastole.

The side-by-side comparison of the average LA global and regional volume-time curves in CTRL and AF groups are shown in Fig. 8. Overall, in AF group LA shows higher volumes compared to CTRL group. Despite such dilation, no significant regional contraction differences were identified between the two groups as shown by the IA (see Table 1).

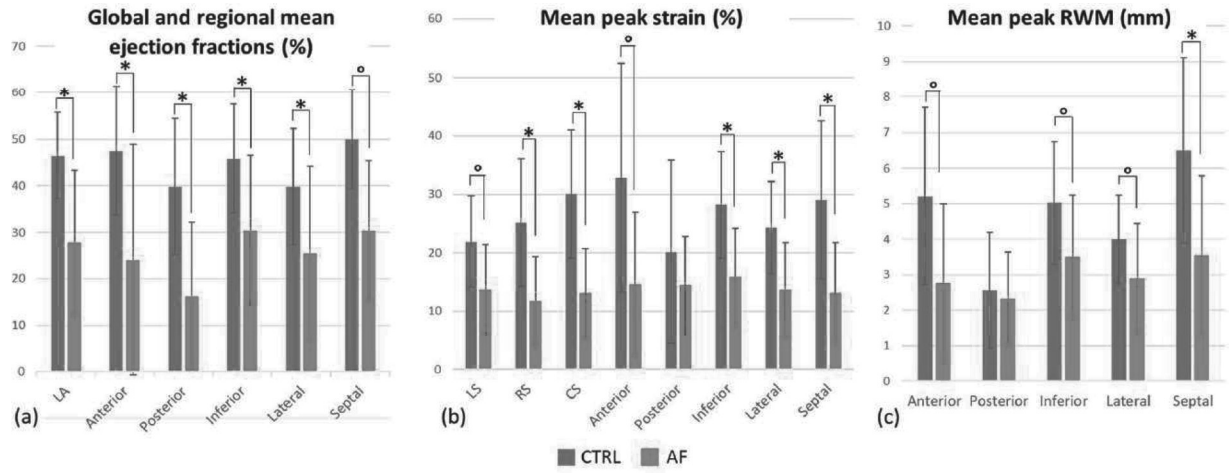

Fig. 9. Mean EF of LA and defined regions of LA (a), Global and regional mean peak strains (b), Mean peak regional wall motion (c).

LA EF and REFs, both measured in the entire LA and in each single region, demonstrated considerably lower values in AF than in CTRL group (see Fig. 9(a)).

Overall, global and regional strain values were higher in CTRL group than in AF group, a fact which accounts for the expected normal function of LA throughout the cardiac cycle in CTRL group (see Table 1 for mean strain values at global and regional level, and Fig. 9(b) for mean peak global strain and mean peak radial strain at distinct regions in the two populations). Global LA strain variation was more evident in the circumferential and radial directions ($p < 0.005$), while regional strain differences were more prominent in RS at the inferior, lateral, and septal regions ($p < 0.005$).

This same behaviour was noticed as regards mean peak RWM (Fig. 9 (c)) which presented higher values in CTRL group in comparison with AF group in every region, apart from the posterior one (Table 1), the widest difference being at the septal region ($p < 0.005$).

On the other hand, mean RSF values were close to each other in both groups, but statistical test was able to identify significant variations in anterior, inferior, lateral, and septal regions ($p < 0.005$) as shown in the table.

Among all the regions, posterior region showed non-significant differences between CTRL group and AF group (Table 1).

Although IA_{RWM} did not show statistically different values ($p = 0.08$) between CTRL and AF groups, RWM curves revealed noticeable irregularities and random regional contractions in some AF patients. To illustrate this finding, in Fig. 10 we show RWM curves of an AF patient alongside a CTRL subject. In CTRL, the peak RWM occurred simultaneously in all regions except in the posterior, whereas in the AF patient a lack of synchronicity in the contraction was evident across all regions.

4. Discussion

Our study presents several points of originality. First, we proposed an automatic approach for regional segmentation of the LA which, as far as we know, would appear the most comprehensive 3D model available nowadays. Whereas regional segmentation of the LV into 17 segments according to a widely accepted guideline [23] is a standard in clinical practice, nothing similar exists as regards LA. Some previous studies have proposed methods which were applied only on conventional LA anatomies having four PVs [24]. Electrogram-based methods for subdividing LA in regions, like those aimed at analysing complex fractionated electrograms [25–28] have led to an excess of heterogeneity in defining the boundaries of the LA regions [29], and have neither been tested on variable anatomies nor correlated with the corresponding regional mechanical behaviour.

Among more recently published works, most [30–40] required the subdivision of the LA surface in regions to focus on specific clinical objectives, for example the modelling of muscle fibres [31,35,36,39], the atrial fibrosis distribution [33,40] to determine the electrophysiological relationship between the atria [34], or the existence of gender-based electrophysiological substrate differences to account for the unfavourable AF ablation outcomes [32]. In these studies, a different number of LA regions were used; for example, in [33,35,36,38,41] only PVs, MV and LAA were labelled, and the LA chamber was considered as one region. In [39] and [31] manual seed points were required and influenced regionalization results. Importantly, in all these studies the regionalization approach was not described, and the reproducibility of their results could be biased by such missing information, given the absence of any guideline and recommendation framework to rely on. In [37], a specific regionalization approach was applied by a commercial software (ADAS 3D, Galgo Medical, Barcelona, Spain) to divide the LA into 13 regions and to allow a 2D atrial mapping: this could make it possible to visualize and interpret intra-subject information and to perform inter-subject comparison, but the method was not open source.

In [40] and [30], the pipeline for LA regionalization was described in detail. In [30], some manual inputs were required to obtain 2D LA flattening maps on which to apply the regionalization to quantitatively assess the correlation between the extents of fibrotic tissue from MRI-late gadolinium enhanced scan and low -voltage areas measured by electro-anatomical mapping. Unfortunately, no assessment of the regionalization approach was provided and neither the code nor the data were made available to perform a quantitative comparison between our and their proposed approach.

Our LA regionalization approach was tested and demonstrated in most of the LA anatomies reported in literature (Fig. 5), suggesting that it is able to cover most anatomical variations of LA, regardless of both PVs number and size and LAA position. Moreover, our approach was completely automatic thus minimizing the influence of the operator on regionalization results and allowing a dynamic LA regionalization. Our methodology showed poor results in 10% of the cases (3 patients), presumably due to the presence of bulges and curves on LA surface. To overcome this limitation, we designed a tool for the manual correction of the points P1, P2, P7 and P8 at the PVs, to finalize the regionalization directly on the LA anatomy into the 3D space.

Secondly, we proposed ten parameters to quantify patient-specific LA mechanical contraction, all of which had been originally devised for LV regional segmentation [21] and were translated into our regionalization process of LA.

In current clinical practice LA contraction is assessed by 2D echocardiography. In our study the contraction parameters were made available also in controls and by 3D CT imaging. The reliability of our results had to be checked by comparing them with other previously

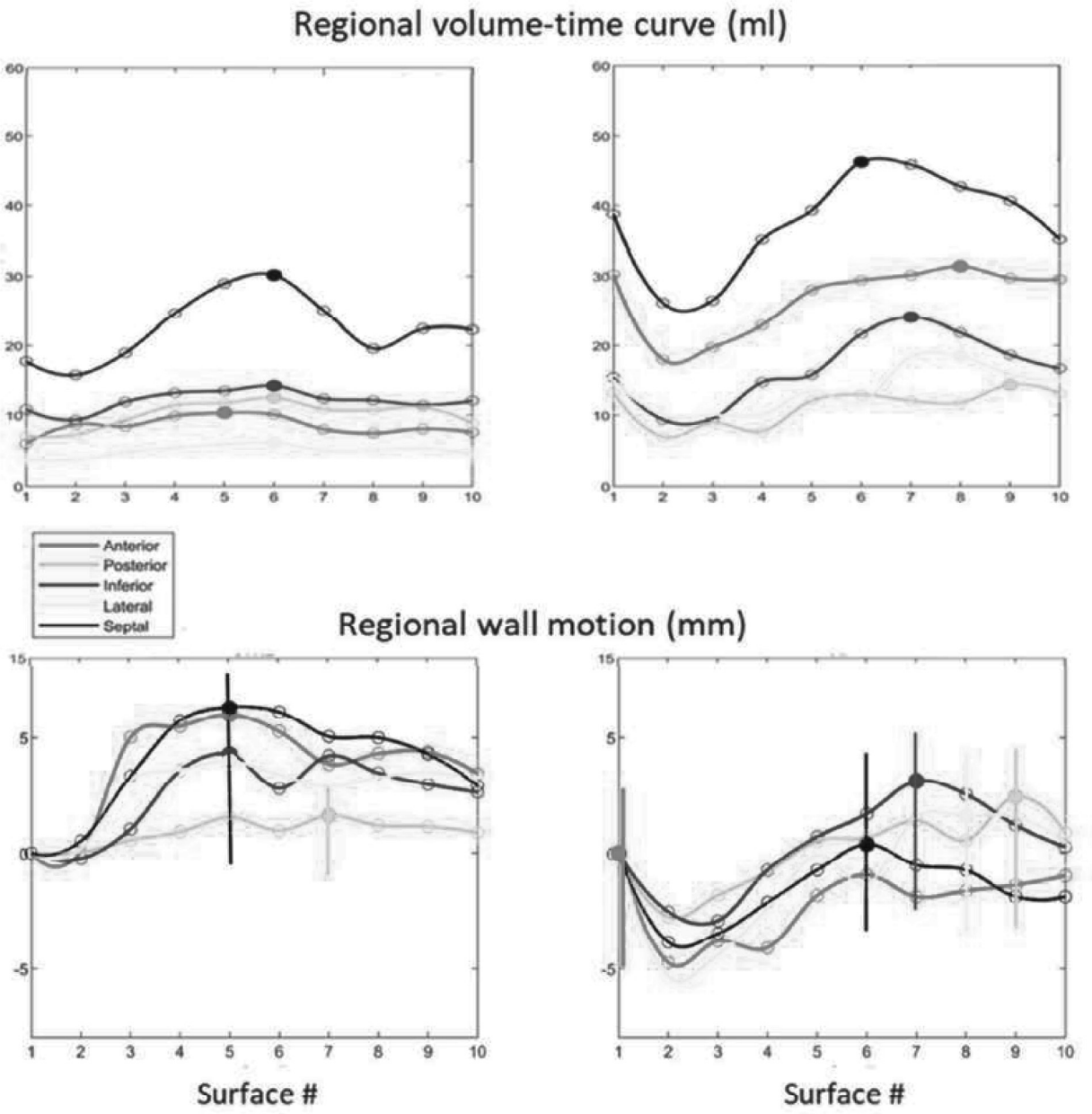

Fig. 10. RWM and regional volume curves for two subjects. RWM peaks have been highlighted with vertical lines to make them more evident.

reported values, mainly derived from echocardiography. Indeed, in [42] longitudinal strain from 3D echocardiography in 105 healthy subjects (median value of age: 42 years) was 23.7 ± 7.6%, which is surprisingly close to the values computed in our CTRL group (21.9 ± 7.9%). In [43], in groups of healthy subjects ($n = 15$) and paroxysmal AF patients with and without LA dilation ($n = 22$ vs $n = 9$) both peak longitudinal and circumferential strain values were measured by 3D speckle tracking echocardiography (3DSTE) and 2D speckle tracking echocardiography (2DSTE). By comparing such results with ours, strain values appeared slightly different (CTRL group - LS: 25.7 ± 7.2% by 3DSTE vs 21.9 ± 7.9%; CS: 37.1 ± 10.2% by 3DSTE vs 30.07 ± 10.96); AF group - LS: 16.0 ± 6.6% by 3DSTE vs 13.7 ± 7.8%, CS: 21.2 ± 13.4% by 3DSTE vs 13.1 ± 7.6%). Differences were probably due to the different imaging modalities and methods applied to compute the strains and might be also due to gender and age differences in the selected populations since our CTRL cohort was slightly older (60.7 ± 10.1 yrs vs 57.9 ± 5.4 yrs), included more males (12 vs 10) and showed higher LA volumes [43]. Given that any deeper investigation was restrained by the low number of subjects in CTRL group, two more comments are to be made: 1) as previously reported in [44], longitudinal strain values might have a wide variability (reported range: 23.0–67.6%); 2) our peak longitudinal strain values in AF patients were closer to 3DSTE, a technique which is considered more sensitive for the detection of LA dysfunction in AF patients as compared to 2DSTE (13.7 ± 7.8% vs 16.0 ± 6.6% (3DSTE) vs 21.2 ± 13.4% (2DSTE)). Taken together, these considerations could support the proposition of our approach for a clinical use in practice.

In addition to strains, in our work several contraction parameters were proposed for patients with AF, and as far as we know, this is the first study to present a quantitative description of the LA contraction alterations associated with a history of AF also at a regional level. Unfortunately, since CT imaging data were acquired in SR in all patients, the cause/effect relationship between LA functional modifications and occurrence of AF cannot be addressed, and we were able to only describe a significant association. On these premises, results in our 17 AF patients highlighted relevant differences in comparison with CTRL as regards: (1) impaired global and regional contraction, the latter being evident in REF

and regional volume as well as in strain values; (2) significantly lower circumferential and radial strain values and (3) worsening of regional contraction parameters in all regions, with the most prominent reduction at the septal region, followed by anterior, inferior, and lateral regions.

Overall, our results showed that: (1) the global impairment of LA contraction associated with AF appears more pronounced along radial and circumferential direction; (2) the more pronounced regional impairment of radial strain in septal, inferior, and lateral regions could point to a more considerable reduction in mechanical efficiency in these regions in comparison to the posterior and anterior ones.

The reduction of mechanical efficiency was also associated with asynchronous contraction underlined by time occurrence of the peaks of the RWM curves in AF patients; in addition, the RWM curves in CTRL and AF groups showed interesting differences in shape, markedly pointing to a time delay in the beginning of atrial diastole. It seemed that at the start of ventricular diastole, the entire process of atrial systole was delayed. Although this observation might be slightly inaccurate due to CT frame rate acquisition, we cannot exclude a slowing down of atrial relaxation in AF condition. This observation needs further investigation in a suitable population.

For research purposes, the computed contraction parameters provided patient-specific boundary conditions for computational fluid-dynamic simulations to investigate thrombogenic events within LA. Indeed, in most of the LA computational fluid dynamic simulation studies, rigid LA surfaces were considered. This approach would appear correct in case of permanent AF patients, where the normal atrial contraction is totally compromised. However, in case of paroxysmal AF patients, it is prone to errors. Our computed contraction parameters can provide patient-specific boundary conditions to convert a rigid domain into a moving domain and support more realistic simulations.

Our study had several limitations. Regarding the methodological approach, measurements of RWM may also be influenced by the definition of long axis of LA. In most cases, the endpoint of long axis lies on the posterior region which consequently evaluated a minimum RWM for posterior region among all other regions and was the least contribution in the global LA contraction. Nonetheless, a similar result came from previous researches where the posterior region was identified as one of the least contributing regions in terms of regional velocity and regional ejection fraction [45]. Once again, an exact comparison was not possible due to the differently defined regional boundaries. In the above-mentioned study, regional volume was defined by projecting boundary points of each region towards the geometrical centre of LA, located inside the LA surface, and then, by tracing the regional volumetric changes at each point of the cycle, the relative contribution of each region in global volume was measured. However, with this strategy, the cumulative sum of the regional volumes at any time frame may escalate from the global LA volume, because an overlapping between regional volumes is a possibility. Instead, in our approach, regional volumes were defined using long axis which is a straight line. With this, each region occupied explicit volume without superimposing with other regions and the total sum of regional volumes at any specific time never exceeded the actual LA volume.

Regarding the current implementation of our approach, although the regionalization algorithm was automatic, manual cut of the PVs and LAA was required. A possibility to overcome this limitation might be offered by the shape diameter function applied in [46], which could be easily integrated into the proposed workflow.

In our study, CT images for each subject were acquired at ventricular end diastole throughout the cardiac cycle. The low temporal resolution is therefore a critical factor that may have affected the precise detection of end diastolic and end systolic phases and consequently our asynchrony indices, which in fact resulted as non-significantly different between the CTRL and AF groups.

5. Conclusion

This study proposes an approach to regionalizing LA chamber and to assessing the region-based mechanical function of LA in controls and AF patients. The regionalization method has been proved to be robust with several LA anatomical variations and also able to characterize contraction changes associated with AF. Testing it on larger dataset may help to evaluate the clinical potential of this methodology.

CRediT authorship contribution statement

Sachal Hussain: Writing – review & editing, Writing – original draft, Validation, Software, Methodology. **Matteo Falanga:** Writing – review & editing, Methodology, Formal analysis, Data curation. **Antonio Chiaravalloti:** Writing – review & editing, Data curation. **Corrado Tomasi:** Writing – review & editing, Validation, Supervision, Conceptualization. **Cristiana Corsi:** Writing – review & editing, Supervision, Methodology, Funding acquisition, Conceptualization.

Declaration of competing interest

The authors declare that they have no known competing financial interests or personal relationships that could have appeared to influence the work reported in this paper.

Acknowledgement

This work was supported by PersonalizeAF project. This project has received funding from the European Union's Horizon 2020 research and innovation programme under the Marie Skłodowska-Curie grant agreement No 860974.

References

[1] B.D. Hoit, Left Atrial Size and Function Role in Prognosis, J. Am. Coll. Cardiol. 63 (6) (2014) 493–505, https://doi.org/10.1016/j.jacc.2013.10.055.
[2] N.M. Al-Saady, O.A. Obel, A.J. Camm, Left atrial appendage: structure, function, and role in thromboembolism, Heart 82 (5) (1999) 547–554, https://doi.org/10.1136/hrt.82.5.547.
[3] G. Lippi, F. Sanchis-Gomar, G. Cervellin, Global epidemiology of atrial fibrillation: an increasing epidemic and public health challenge, Int. J. Stroke 16 (2) (2021) 217–221, https://doi.org/10.1177/1747493019897870.
[4] L.E. Henault, et al., Prevalence of Diagnosed Atrial Fibrillation in Adults, Jama 285 (18) (2003) 2370.
[5] N.F. Murphy, et al., A national survey of the prevalence, incidence, primary care burden and treatment of atrial fibrillation in Scotland, Heart 93 (5) (2007) 606–612, https://doi.org/10.1136/hrt.2006.107573.
[6] J.N. Ruskin, J.P. Singh, Atrial fibrillation endpoints: hospitalization, Hear. Rhythm 1 (2) (2004) 31–35, https://doi.org/10.1016/j.hrthm.2004.04.004. SUPPL.
[7] M. Santini, et al., Atrial fibrillation requiring urgent medical care. Approach and outcome in the various departments of admission. Data from the atrial Fibrillation/flutter Italian REgistry (FIRE), Ital. Hear. J. 5 (3) (2004) 205–213.
[8] R.S. Phang, et al., Echocardiographic evidence of left atrial abnormality in young patients with lone paroxysmal atrial fibrillation, Am. J. Cardiol. 94 (4) (2004) 511–513, https://doi.org/10.1016/j.amjcard.2004.05.009.
[9] D.P. Zipes, Atrial fibrillation: from cell to bedside, J. Cardiovasc. Electrophysiol. 8 (8) (1997) 927–938, https://doi.org/10.1111/j.1540-8167.1997.tb00855.x.
[10] A. Nemes, P. Domsik, A. Kalapos, T. Forster, Is three-dimensional speckle-tracking echocardiography able to identify different patterns of left atrial dysfunction in selected disorders?: short summary of the MAGYAR-Path Study, Int. J. Cardiol. 220 (2016) 535–537, https://doi.org/10.1016/j.ijcard.2016.06.122.
[11] K. Havasi, et al., Left Atrial Deformation Analysis in Patients with Corrected Tetralogy of Fallot by 3D Speckle-Tracking Echocardiography (from the MAGYAR-Path Study), Arq. Bras. Cardiol. 108 (2) (2017) 129–134, https://doi.org/10.5935/abc.20170004.
[12] P. Reant, et al., Reverse remodeling of the left cardiac chambers after catheter ablation after 1 year in a series of patients with isolated atrial fibrillation, Circulation 112 (19) (2005) 2896–2903, https://doi.org/10.1161/CIRCULATIONAHA.104.523928.
[13] M. Nuñez-Garcia, G. Bernardino, R. Doste, J. Zhao, O. Camara, C. Butakoff, C., Standard Quasi-Conformal Flattening of the Right and Left Atria. In: Coudière, Y., Ozenne, V., Vigmond, E., Zemzemi, N. (eds) Functional Imaging and Modeling of the Heart. FIMH 2019. Lecture Notes in Computer Science, vol 11504. Springer, Cham. 10.1007/978-3-030-21949-9_10.

[14] R. Karim, et al., Surface flattening of the human left atrium and proof-of-concept clinical applications, Comput. Med. Imaging Graph. 38 (4) (2014) 251–266, https://doi.org/10.1016/j.compmedimag.2014.01.004.
[15] L.C. Prasanna, R. Praveena, A.S. D'Souza, K.M.R. Bhat, Variations in the pulmonary venous ostium in the left atrium and its clinical importance, J. Clin. Diagnostic Res. 8 (2) (2014) 10–11, https://doi.org/10.7860/JCDR/2014/7649.3992.
[16] C.B. Moyer, et al., Wall-motion based analysis of global and regional left atrial mechanics, IEEE Trans. Med. Imaging 32 (10) (2013) 1765–1776, https://doi.org/10.1109/TMI.2013.2264062.
[17] T.F. Chan, L.A. Vese, Active contours without edges, IEEE Trans. Image Process. 10 (2) (2001) 266–277, https://doi.org/10.1109/83.902291.
[18] Autodesk Meshmixer, "Meshmixer 3.5," 2018. https://www.meshmixer.com.
[19] R. Kato, et al., Pulmonary vein anatomy in patients undergoing catheter ablation of atrial fibrillation: lessons learned by use of magnetic resonance imaging, Circulation 107 (15) (2003) 2004–2010, https://doi.org/10.1161/01.CIR.0000061951.81767.4E.
[20] W. Wang, D. Buehler, A. Hamzei, X. Wang, X. Yuan, Comprehensive surgical approach to treat atrial fibrillation in patients with variant pulmonary venous anatomy, J. Thorac. Cardiovasc. Surg. 145 (3) (2013) 790–795, https://doi.org/10.1016/j.jtcvs.2012.03.019.
[21] C. Corsi, et al., Volumetric quantification of global and regional left ventricular function from real-time three-dimensional echocardiographic images, Circulation 112 (8) (2005) 1161–1170, https://doi.org/10.1161/CIRCULATIONAHA.104.513689.
[22] L. Chen, et al., Left atrial strain measured by 4D Auto LAQ echocardiography is significantly correlated with high risk of thromboembolism in patients with non-valvular atrial fibrillation, Quant. Imaging Med. Surg. 11 (9) (2021) 3920–3931, https://doi.org/10.21037/qims-20-1381.
[23] M.D. Cerqueira, et al., Standardized myocardial sementation and nomenclature for tomographic imaging of the heart: a Statement for Healthcare Professionals from the Cardiac Imaging Committee of the Council on Clinical Cardiology of the American Heart Association, Circulation 105 (4) (2002) 539–542, https://doi.org/10.1161/hc0402.102975.
[24] S.E. Williams, et al., Standardized unfold mapping: a technique to permit left atrial regional data display and analysis, J. Interv. Card. Electrophysiol. 50 (1) (2017) 125–131, https://doi.org/10.1007/s10840-017-0281-3.
[25] Y. Hori, et al., Influence of left atrium anatomical contact area in persistent atrial fibrillation - Relationship between low-voltage area and fractionated electrogram, Circ. J. 78 (8) (2014) 1851–1857, https://doi.org/10.1253/circj.CJ-14-0440.
[26] A.W. Teh, et al., Electroanatomic remodeling of the left atrium in paroxysmal and persistent atrial fibrillation patients without structural heart disease, J. Cardiovasc. Electrophysiol. 23 (3) (2012) 232–238, https://doi.org/10.1111/j.1540-8167.2011.02178.x.
[27] R.J. Hunter, et al., Characterization of fractionated atrial electrograms critical for maintenance of atrial fibrillation a randomized, controlled trial of ablation strategies (the CFAE AF trial, Circ. Arrhythmia Electrophysiol. 4 (5) (2011) 622–629, https://doi.org/10.1161/CIRCEP.111.962928.
[28] Y.L. Chen, J.E. Ban, Y.M. Park, J. Il Choi, S.W. Park, Y.H. Kim, The spatial distribution of atrial fibrillation termination sites in the right atrium during complex fractionated atrial electrograms-guided ablation in patients with persistent atrial fibrillation, J. Cardiovasc. Electrophysiol. 24 (9) (2013) 949–957, https://doi.org/10.1111/jce.12187.
[29] R. Starreveld, L.J.M.E. Van Der Does, N.M.S. De Groot, Anatomical hotspots of fractionated electrograms in the left and right atrium: do they exist? Eur. Soc. Cardiol. 21 (1) (2019) 60–72, https://doi.org/10.1093/europace/euy059.
[30] Y. Coudière, V. Ozenne, D. Hutchison, Functional Imaging and Modeling of the Heart 2019 Proceedings, 2019. June.
[31] A. Wachter, A. Loewe, M.W. Krueger, O. Dössel, G. Seemann, Mesh structure-independent modeling of patient-specific atrial fiber orientation, Curr. Dir. Biomed. Eng. 1 (1) (2015) 409–412, https://doi.org/10.1515/cdbme-2015-0099.
[32] G.R. Wong, et al., Sex-Related Differences in Atrial Remodeling in Patients with Atrial Fibrillation: relationship to Ablation Outcomes, Circ. Arrhythmia Electrophysiol. 15 (1) (2022) E009925, https://doi.org/10.1161/CIRCEP.121.009925.
[33] O. Razeghi, et al., Fully Automatic Atrial Fibrosis Assessment Using a Multilabel Convolutional Neural Network, Circ. Cardiovasc. Imaging 13 (12) (2020) E011512, https://doi.org/10.1161/CIRCIMAGING.120.011512.
[34] S. Prabhu, et al., A comparison of the electrophysiologic and electroanatomic characteristics between the right and left atrium in persistent atrial fibrillation: is the right atrium a window into the left? J. Cardiovasc. Electrophysiol. 28 (10) (2017) 1109–1116, https://doi.org/10.1111/jce.13297.
[35] R. Piersanti, et al., Modeling cardiac muscle fibers in ventricular and atrial electrophysiology simulations, Comput. Methods Appl. Mech. Eng. 373 (2021) 113468, https://doi.org/10.1016/j.cma.2020.113468.
[36] J.A. Solís-Lemus, et al., Evaluation of an open-source pipeline to create patient-specific left atrial models: a reproducibility study, Comput. Biol. Med. 162 (2023) 107009, https://doi.org/10.1016/j.compbiomed.2023.107009. May.
[37] T. Wang, et al., Standardized 2D atrial mapping and its clinical applications, Comput. Biol. Med. 168 (2024) 107755, https://doi.org/10.1016/j.compbiomed.2023.107755. November 2023.
[38] L. Azzolin, et al., AugmentA: patient-specific augmented atrial model generation tool, Comput. Med. Imaging Graph. 108 (2023), https://doi.org/10.1016/j.compmedimag.2023.102265. September 2022.
[39] A.L. Tianbao Zheng, Luca Azzolin, Jorge Sánchez, Olaf Dössel, An automate pipeline for generating fiber orientation and region annotation in patient specific atrial models, Curr. Dir. Biomed. Eng. 2003 (2) (2007) 1–25.
[40] C. Goetz, et al., Discrepancy between LGE-MRI and electro-anatomical mapping for regional detection of pathological atrial substrate, Curr. Dir. Biomed. Eng. 9 (1) (2023) 483–486, https://doi.org/10.1515/cdbme-2023-1121.
[41] C.H. Roney, et al., Universal atrial coordinates applied to visualisation, registration and construction of patient specific meshes, Med. Image Anal. 55 (2019) 65–75, https://doi.org/10.1016/j.media.2019.04.004.
[42] Y. Nabeshima, T. Kitano, M. Takeuchi, Reliability of left atrial strain reference values: a 3D echocardiographic study, PLoS One 16 (4) (2021) 1–18, https://doi.org/10.1371/journal.pone.0250089. April.
[43] A. Mochizuki, et al., Assessment of left atrial deformation and synchrony by three-dimensional speckle-tracking echocardiography: comparative studies in healthy subjects and patients with atrial fibrillation, J. Am. Soc. Echocardiogr. 26 (2) (2013) 165–174, https://doi.org/10.1016/j.echo.2012.10.003.
[44] A.B. Nielsen, et al., Normal values and reference ranges for left atrial strain by speckle-tracking echocardiography: the Copenhagen City Heart Study, Eur. Heart J. Cardiovasc. Imaging 23 (1) (2022) 42–51, https://doi.org/10.1093/ehjci/jeab201.
[45] P. Kuklik, et al., Quantitative description of the 3D regional mechanics of the left atrium using cardiac magnetic resonance imaging, Physiol. Meas. 35 (5) (2014) 763–775, https://doi.org/10.1088/0967-3334/35/5/763.
[46] A. Masci, L. Barone, L. Dedè, M. Fedele, C. Tomasi, and C.P. Bradley, "The impact of left atrium appendage morphology on stroke risk assessment in atrial fibrillation : a computational fluid dynamics study," vol. 9, no. January, pp. 1–11, 2019, 10.3389/fphys.2018.01938.